2p photoelectron spectra and linear alignment dichroism of atomic Cr

Ph. Wernet,* J. Schulz, and B. Sonntag
II. Institut für Experimentalphysik, Universität Hamburg, Luruper Chaussee 149, D-22761 Hamburg, Germany

K. Godehusen and P. Zimmermann
Institut für Atomare und Analytische Physik, Technische Universität Berlin, Hardenbergstrasse 36, D-10623 Berlin, Germany

A. N. Grum-Grzhimailo
Institute of Nuclear Physics, Moscow State University, 119899 Moscow, Russia

N. M. Kabachnik†
Fakultät für Physik, Universität Bielefeld, D-33615 Bielefeld, Germany

M. Martins
Institut für Experimentalphysik, Freie Universität Berlin, Arnimallee 14, D-14195 Berlin, Germany
(Received 21 February 2001; published 12 September 2001)

The 2p photoionization of free Cr atoms has been studied. Unpolarized as well as laser-aligned Cr atoms have been ionized with linearly polarized undulator radiation well above the 2p ionization thresholds. The investigation of the main and satellite 2p photoelectron lines and of the linear alignment dichroism allowed for a detailed characterization of the Cr 2p photoionization process. The spectra are compared to the predictions of the pure jK coupling model and to the results of intermediate coupling Hartree-Fock calculations. The importance of the investigations for the discussion of the 2p photoelectron spectra of bound 3d transition-metal atoms is pointed out.

DOI: 10.1103/PhysRevA.64.042707 PACS number(s): 32.80.Fb, 32.80.Hd

I. INTRODUCTION

The dichroism in the photoelectron spectra of polarized atoms is defined as the intensity difference for two different directions either of the target atom polarization or of the polarization of the ionizing photons. The interest in investigating the dichroism in the photoelectron spectra of free atoms is twofold. First, a comparison of the dichroism of free oriented atoms to the dichroism of magnetized solid samples can help in the assessment of intra-atomic and interatomic effects in the spectra of bound atoms. Second, the investigation of dichroism allows for a detailed probing of the dynamics of the photoionization process of the free atoms since it gives access to the amplitudes and phases of the dipole matrix elements [1]. The most commonly performed dichroism measurements on free atoms are the linear magnetic dichroism in the angular distribution (LMDAD) and the linear alignment dichroism (LAD) ([2], and references therein). The LMDAD is measured with linearly polarized ionizing light for two mutually antiparallel directions of the atomic polarization whereby only the atomic orientation (and not the alignment) contributes. The LAD is measured with linearly polarized ionizing light but for two mutually perpendicular directions of the target atom alignment.

In earlier investigations, the dichroism in the subvalence photoelectron spectra of ground-state laser polarized 3d transition-metal and 4f rare-earth atoms has been investigated well-above threshold. The 3p photoelectron spectra of Cr atoms [3–5] and the 4f and 5p photoelectron spectra of Eu atoms [6–8] are dominated by the direct and exchange Coulomb interactions. Spin-orbit effects can be neglected except for the fine-structure splitting. An interpretation of the photoelectron and dichroism spectra based on the LSJ coupling approximation is therefore well suited. Very general properties of the dichroism such as the spectral distribution of dichroism as a function of the photoelectron energy (dichroism patterns) and the dichroism integrated over one or several final ionic LSJ multiplets (sum rules) have been derived recently [2].

For the deep core-level 2p photoionization of 3d metal atoms the situation is expected to be completely different. The 2p spin-orbit interaction dominates the spectrum and therefore the inappropriate LSJ coupling approximation should be replaced by a description based on jj or jK coupling. To shed light on this, we present an investigation of the 2p photoelectron spectra of free unpolarized and laser aligned Cr atoms as the key part of a systematic study of the 2p photoelectron spectra of 3d transition-metal atoms.

The investigation of the 2p photoelectron spectrum of Cr is a rewarding task since the theoretical description is simplified due to the half filled $3d^5$ shell of the atom in the ground-state Cr $2p^6 3d^5 4s(^7S)$. Experimentally, in comparison to other 3d metals there are two advantages: (i) Cr sublimes at crucible temperatures of $\sim$1700 K [9] and (ii) free Cr atoms can be effectively polarized by laser pumping [3,10].

*Present address: Stanford Synchrotron Radiation Laboratory, MS 69, 2575 Sand Hill Rd., Menlo Park, CA 94025.

†On leave from Institute of Nuclear Physics, Moscow State University, 119899 Moscow, Russia.

The first part of this paper presents an application of the general theory of the angular distribution of photoelectrons from polarized atoms [11] to the case of pure jj and jK coupling suitable for deep core-level photoelectron spectra (Sec. II). The main interest is focused on the $2p$ photoelectron spectra of the $3d$ transition-metal atoms but the description should also be appropriate for the $3d$ photoelectron spectra of the rare-earth elements. In Sec. III, the experimental setup is described and in Sec. IV, the results on $2p$ photoelectron spectra of unpolarized (Sec. IV A) and aligned free Cr atoms (Sec. IV B) are discussed. The LAD in the $2p$ photoelectron spectra of the polarized Cr atoms is interpreted with the aid of different theoretical approaches. The corresponding results for the LMDAD have been published recently [12]. Finally, information on the dynamics of the photoionization process is extracted from the normalized dichroism spectra (Sec. IV C).

II. THEORY

A. Generalized anisotropy coefficients in pure coupling approximations

The general theoretical treatment of the dichroism in photoionization of polarized atoms has been described in detail in Ref. [2] and is summarized for convenience in the Appendix. We concentrate here on the shape of the dichroism spectra, which is solely determined by the generalized anisotropy coefficients $B_{k_0 k k_\gamma}$, Eq. (A3), and their dependence on the photoelectron energy. In general, the coefficients $B_{k_0 k k_\gamma}$ have a very complex structure. They contain the dipole amplitudes and can only be obtained with the aid of numerical methods. In the analysis of the experimental data (Sec. IV), we calculate the dipole amplitudes and then, using Eq. (A3), the coefficients $B_{k_0 k k_\gamma}$ within the Hartree-Fock (HF) approximation in intermediate coupling. However, for a qualitative discussion and for a better understanding of the influence of various factors on the shape of the dichroism spectra, it is instructive to consider the dipole amplitudes within an approximation of pure coupling schemes. In this case, Eq. (A3) can be simplified considerably and allows us to predict general regularities for the dichroism in the core-level photoelectron spectra without explicit knowledge of the dipole amplitudes. An example of such an analysis has been presented in [2] within the LSJ coupling approximation. In deep, core-level photoionization the spin-orbit splitting of the core hole dominates the photoelectron spectrum and therefore the jj or jK coupling approximations are more appropriate.

Consider the photoionization proceeding according to one of the schemes

$$\alpha_0 J_0 + \hbar\omega \rightarrow [[\alpha_f (l_0 j_0)^{-1}, J_0 : J_f] + \varepsilon l j] J \quad (jj \text{ coupling}), \tag{1}$$

or

$$\alpha_0 L_0 S_0 J_0 + \hbar\omega \rightarrow [[\alpha_f (l_0 j_0)^{-1}, L_0 [K_f] S_0 : J_f] + \varepsilon l j] J \quad (jK \text{ coupling}). \tag{2}$$

The initial (final) state of the atom (ion) is characterized by the total angular momentum $J_0 (J_f)$ and other quantum numbers $\alpha_0 (\alpha_f)$. The photoelectron has a kinetic energy ε and the orbital and total angular momenta l and j. The total angular momentum of the final system consisting of the ion and the photoelectron is denoted by J. In the dipole approximation, well justified in the present study, the values for J are given by $J = J_0, J_0 \pm 1$.

We imply a single-configuration approximation. The initial atomic state is described by only one electron configuration and the final ion electron configuration is obtained from the initial one by removing one electron from an inner closed core shell $n_0 l_0$. The core hole is assumed to be well described by the total angular momentum $j_0 = l_0 \pm 1/2$ due to its large spin-orbit interaction. The valence shells are kept frozen. This means that all quantum numbers of the valence shells in the initial atom and in the photoion are identical. Equation (1) corresponds to the jj coupling approximation in the description of the photoion, i.e., j_0 is coupled to the total angular momentum J_0 of the valence shells resulting in the total angular momentum J_f of the photoion. This coupling scheme is applicable if the spin-orbit interaction in the valence shell is much stronger than the Coulomb interaction between the hole and the valence electrons. Equation (2) corresponds to the jK coupling approximation [13] (sometimes also called jl coupling, see e.g. [14]), which is valid in the other limiting case when the spin-orbit interactions of the valence electrons are much weaker than the core-valence Coulomb interaction. In this case, the angular momentum of the hole j_0 is first coupled to the orbital angular momentum of the valence electrons L_0 resulting in the angular momentum K_f, which then couples with the total spin of the valence shell S_0 to the total angular momentum of the ion J_f. Naturally, in the latter case, the initial state of the atom should be well described in the LSJ coupling scheme. The above jj and jK coupling approximations contrast with the LSJ coupling approximation for the subvalence spectra in Ref. [2] where the spin-orbit interactions both for the hole and for the valence electrons were assumed much weaker than the Coulomb hole-valence interaction.

Within the single-configuration, frozen valence shell, and pure coupling scheme approximations the dipole amplitudes in Eq. (A3) can be reduced according to the expressions

$$\langle \alpha_f J_f, \varepsilon l j : J \| D \| \alpha_0 J_0 \rangle \equiv \langle j_0^{-1} J_0 : J_f, \varepsilon l j : J \| D \| \alpha_0 J_0 \rangle = \hat{J} \hat{J}_f (-1)^{J + j_0 + J_f + 1} \begin{Bmatrix} J_0 & j_0 & J_f \\ j & J & 1 \end{Bmatrix} \times \langle \varepsilon l j \| d \| j_0 \rangle \quad (jj \text{ coupling}) \tag{3}$$

or

$$\langle \alpha_f J_f, \varepsilon lj:J \| D \| \alpha_0 J_0 \rangle$$
$$\equiv \langle j_0^{-1} L_0(K_f), S_0 : J_f, \varepsilon lj:J \| D \| \alpha_0 (L_0 S_0) J_0 \rangle$$
$$= \hat{J}\hat{K}_f \hat{J}_0 \hat{J}_f (-1)^{2J_0+L_0+S_0+J-1} \begin{Bmatrix} j_0 & L_0 & K_f \\ S_0 & J_f & J_0 \end{Bmatrix}$$
$$\times \begin{Bmatrix} J_0 & j_0 & J_f \\ j & J & 1 \end{Bmatrix} \langle \varepsilon lj \| d \| j_0 \rangle \quad (jK \text{ coupling}). \quad (4)$$

We use the standard notations for the Wigner nj coefficients and $\hat{J} \equiv (2J+1)^{1/2}$. The reduced matrix elements $\langle \varepsilon lj \| d \| j_0 \rangle$ contain the one-electron wave functions of the core hole and of the photoelectron only.

If the single-electron matrix elements are independent of the total angular momentum quantum numbers, then after substitution of Eqs. (3) or (4) into Eq. (A3), the summation over the angular momenta J and J' can be performed analytically (see, e.g., [15]). This results in

$$B_{k_0 k k_\gamma} = \tilde{C}_{k_0}(j_0, J_f) \tilde{b}_{k_0 k k_\gamma}(j_0) \quad (jj \text{ coupling}) \quad (5)$$

or

$$B_{k_0 k k_\gamma} = \tilde{C}_{k_0}(j_0, K_f, J_f) \tilde{b}_{k_0 k k_\gamma}(j_0) \quad (jK \text{ coupling}), \quad (6)$$

where

$$\tilde{C}_{k_0}(j_0, K_f, J_f) = 3\hat{J}_0^3 \hat{K}_f^2 \hat{j}_f^2 (-1)^{k_\gamma + k + k_0 + J_f + J_0 + j_0}$$
$$\times \begin{Bmatrix} j_0 & j_0 & k_0 \\ J_0 & J_0 & J_f \end{Bmatrix} \begin{Bmatrix} J_0 & L_0 & S_0 \\ K_f & J_f & j_0 \end{Bmatrix}^2, \quad (7)$$

$$\tilde{C}_{k_0}(j_0, J_f) = \sum_{K_f} \tilde{C}_{k_0}(j_0, K_f, J_f)$$
$$= 3\hat{J}_0 \hat{j}_f^2 (-1)^{k_\gamma + k + k_0 + J_f + J_0 + j_0}$$
$$\times \begin{Bmatrix} j_0 & j_0 & k_0 \\ J_0 & J_0 & J_f \end{Bmatrix}, \quad (8)$$

and

$$\tilde{b}_{k_0 k k_\gamma}(j_0) = \sum_{l l' j j'} (-1)^{-j' - 1/2} \hat{j}\hat{j}' \hat{l}\hat{l}' (l0, l'0 | k0)$$
$$\times \begin{Bmatrix} j & l & \frac{1}{2} \\ l' & j' & k \end{Bmatrix} \begin{Bmatrix} j_0 & j' & 1 \\ j_0 & j & 1 \\ k_0 & k & k_\gamma \end{Bmatrix} \langle \varepsilon lj \| d \| j_0 \rangle$$
$$\times \langle \varepsilon l' j' \| d \| j_0 \rangle^*. \quad (9)$$

Thus, according to Eqs. (5) and (6), the coefficients $B_{k_0 k k_\gamma}$ may be presented as the product of two factors. The coefficients $\tilde{C}_{k_0}(j_0, J_f)$ and $\tilde{C}_{k_0}(j_0, K_f, J_f)$ contain the coupling of the angular momenta in the final ion for the cases of jj and jK couplings, respectively. They are independent of the dynamics of the photoionization process that is determined by the quantities $\tilde{b}_{k_0 k k_\gamma}(j_0)$ in Eq. (9) through the dipole matrix elements $\langle \varepsilon lj \| d \| j_0 \rangle$. Naturally, for $L_0 = 0$ (atoms with S symmetry) the coefficients (7) and (8) become identical: in this case $J_0 = S_0$ and there is no difference between jj and jK coupling. We note also that within the above approximations, the summation of the coefficients $B_{k_0 k k_\gamma}$ over the quantum number K_f leads to the result identical with the result obtained for jj coupling [see first part of Eq. (8)].

B. Dichroism spectral patterns and sum rules

The shape of the dichroism spectra is directly determined by the coefficients $B_{k_0 k k_\gamma}$. The product form of the coefficients $B_{k_0 k k_\gamma}$ discussed in Sec. II A has important consequences for the description of the dichroism [2]. Far from resonances, the dipole matrix elements $\langle \varepsilon lj \| d \| j_0 \rangle$ only slowly vary with the photoelectron energy. Therefore, the coefficients $\tilde{b}_{k_0 k k_\gamma}(j_0)$ can be considered as being approximately constant over the photoelectron energy range of each multiplet associated with the core hole $(l_0 j_0)^{-1}$. The shape of the corresponding dichroism spectra is thus solely given by the coupling coefficients $\tilde{C}_{k_0}(j_0, K_f, J_f)$ and $\tilde{C}_{k_0}(j_0, J_f)$, Eqs. (7) and (8) provided the energies of the fine-structure levels in the multiplet are known. By considering the dependence of these coefficients on the fine-structure quantum numbers K_f and J_f, general spectral dichroism patterns and dichroism sum rules can be derived in the same way as in [2]. For example, the structure of the $6j$ symbol with two pairs of equal angular momenta in Eq. (8) (jj coupling) is similar to the structure of the corresponding $6j$ symbol in the equations for the coefficients $C_{k_0}(J_0, J_f)$ [Eqs. (15) and (35) from [2]]. Therefore, in complete analogy with the analysis in [2], this $6j$ symbol as a function of J_f shows k_0 zeros. Consequently, in jj coupling for each multiplet $(j_0 = l_0 + 1/2, J_f)$ and $(j_0 = l_0 - 1/2, J_f)$, in case the fine-structure J_f components are arranged in a regular (ascending or descending) way on the energy axis, the number of zeros in the partial dichroism spectrum, associated with a particular statistical tensor $\mathcal{A}_{k_0 0}$, is equal to the rank k_0 of the respective tensor. In many cases, the lowest-order statistical tensors, $\mathcal{A}_{10}$ for orientation and $\mathcal{A}_{20}$ for alignment, are much larger than others (see Sec. III). Disregarding the small contributions of higher-order tensors, one obtains the following properties of the dichroism spectra: the energy dependence of the magnetic dichroism connected with orientation [circular magnetic dichroism (CMD) and LMDAD] shows one zero crossing in each j_0 multiplet of the core-level photoelectron spectrum; the linear alignment dichroism (LAD) shows two zero crossings in each j_0 multiplet of the core-level photoelectron spectrum. The above statement on the dichroism spectra is not as universal as in the LSJ coupling approximation, for which the regular order of the fine-structure components in a multiplet is more strictly governed by the Hund's rule.

The same properties of the dichroism spectra exist in the jK coupling approximation provided the fine structure in J_f is not resolved experimentally. This follows from the relation

$$\sum_{J_f} \tilde{C}_{k_0}(j_0,K_f,J_f) = 3\hat{J}_0^3\hat{K}_f^2(-1)^{k_\gamma+k+j_0+J_0+S_0+K_f} \times \begin{Bmatrix} j_0 & j_0 & k_0 \\ L_0 & L_0 & K_f \end{Bmatrix} \begin{Bmatrix} J_0 & J_0 & k_0 \\ L_0 & L_0 & S_0 \end{Bmatrix}, \tag{10}$$

where the first $6j$ symbol on the right side shows the same behavior as a function of K_f as the one in Eq. (8) as a function of J_f.

Sum rules describe the results obtained upon integrating the dichroism spectra over the photoelectron energy. Within the above approximations integrating over the range of one j_0 multiplet is equivalent to the summation of the coefficient $\tilde{C}_{k_0}(j_0,K_f,J_f)$ in Eq. (7) over J_f, K_f in the jK coupling approximation or to the summation of the coefficient $\tilde{C}_{k_0}(j_0,J_f)$ in Eq. (8) over J_f in the jj coupling approximation. The summations give

$$\sum_{J_f K_f} \tilde{C}_{k_0}(j_0,K_f,J_f) = \sum_{J_f} \tilde{C}_{k_0}(j_0,J_f) = 3\hat{J}_0^2\hat{j}_0\delta_{k_0 0}, \tag{11}$$

[note that $k=k_\gamma$ in case $k_0=0$ according to the triangle rule in the $9j$ symbol in Eq. (9)]. Since the dichroism is related to terms with $k_0 \neq 0$, we arrive at the following sum rule: For ionization of an inner-closed $(l_0 j_0)$ subshell of an atom with arbitrary total angular momentum the dichroism (LMDAD and LAD) vanishes, upon integration over the part of the photoelectron spectrum associated with the vacancy $(l_0 j_0)^{-1}$.

Evidently the sum rule does not depend on the relative position of the fine-structure components of the $(l_0 j_0)^{-1}$ core hole. As a trivial consequence, the dichroism integrated over the whole photoelectron spectrum vanishes [16]. Remember that we derived this sum rule within pure coupling schemes and implying single configuration and frozen valence-shell approximations.

C. Nonrelativistic approximation of the dipole matrix elements

In order to compare the dichroism in the two different spin-orbit split multiplets ($j_0 = l_0 \pm 1/2$) we introduce a nonrelativistic approximation for the one-electron wave functions of the core hole $(l_0 j_0)$ and of the photoelectron $\varepsilon l j$. Since these wave functions are assumed to be independent of the values of the angular momenta j_0 and j, the dipole matrix elements $\langle \varepsilon l j \| d \| j_0 \rangle$ in Eq. (9) can be further reduced:

$$\langle \varepsilon l j \| d \| j_0 \rangle = \hat{j}\hat{j}_0(-1)^{j_0+l-1/2} \begin{Bmatrix} j_0 & l_0 & \frac{1}{2} \\ l & j & 1 \end{Bmatrix} \langle \varepsilon l \| d \| l_0 \rangle. \tag{12}$$

Equation (12) can be used for not too heavy atoms and for photoionization far from Cooper minima. Upon substituting Eq. (12) into Eq. (9), the summation over the angular momenta j and j' can be performed analytically. The expressions for the coefficients $B_{k_0 k k_\gamma}$ take the form

$$B_{k_0 k k_\gamma} = C_{k_0}(j_0,K_f,J_f) b_{k_0 k k_\gamma} \quad (jK \text{ coupling}), \tag{13}$$

$$B_{k_0 k k_\gamma} = C_{k_0}(j_0,J_f) b_{k_0 k k_\gamma} \quad (jj \text{ coupling}), \tag{14}$$

where

$$C_{k_0}(j_0,K_f,J_f) = 3\hat{J}_0^3\hat{K}_f^2\hat{J}_f^2\hat{j}_0^2(-1)^{J_f+J_0+l_0+k_0-1/2} \times \begin{Bmatrix} j_0 & j_0 & k_0 \\ l_0 & l_0 & \frac{1}{2} \end{Bmatrix} \begin{Bmatrix} j_0 & j_0 & k_0 \\ J_0 & J_0 & J_f \end{Bmatrix} \times \begin{Bmatrix} J_0 & L_0 & S_0 \\ K_f & J_f & j_0 \end{Bmatrix}^2, \tag{15}$$

$$C_{k_0}(j_0,J_f) = \sum_{K_f} C_{k_0}(j_0,K_f,J_f) = 3\hat{J}_0\hat{J}_f^2\hat{j}_0^2(-1)^{J_f+J_0+l_0+k_0-1/2} \times \begin{Bmatrix} j_0 & j_0 & k_0 \\ l_0 & l_0 & \frac{1}{2} \end{Bmatrix} \begin{Bmatrix} j_0 & j_0 & k_0 \\ J_0 & J_0 & J_f \end{Bmatrix}, \tag{16}$$

and

$$b_{k_0 k k_\gamma} = \sum_{ll'} (-1)^l \hat{l}\hat{l}'(l0,l'0|k0) \begin{Bmatrix} l_0 & l & 1 \\ l_0 & l' & 1 \\ k_0 & k & k_\gamma \end{Bmatrix} \langle \varepsilon l \| d \| l_0 \rangle \times \langle \varepsilon l' \| d \| l_0 \rangle^*. \tag{17}$$

A similar reduction for photoionization of the Rydberg electron was considered by Cherepkov (quoted in [17]) for the case of jK coupling in the initial excited atomic state and the final ion state without a hole. The one-electron parameters $b_{k_0 k k_\gamma}$ in Eq. (17) are equal to the ones introduced in Ref. [2]. The product form of the coefficients $B_{k_0 k k_\gamma}$ of course persists and consequently, all properties of the dichroism spectra and sum rules considered above. An additional restriction follows in the nonrelativistic approximation for the one-electron dipole matrix elements from the triangle rule $k_0 \leqslant 2j_0$ in Eqs. (15) and (16): the LAD vanishes for the hole with $j_0 = 1/2$ ($p_{1/2}$ hole for p ionization). Furthermore, a triangle rule for the $9j$ symbol in Eq. (17) requires $k_0 \leqslant 2l_0$ and therefore, within the nonrelativistic approximation, only the lowest statistical tensors $\mathcal{A}_{10}$ and $\mathcal{A}_{20}$ contribute to the dichroism in $2p$ core-level photoelectron spectra [18].

Finally, in addition to the spectral patterns and sum rules, a relative sign of the magnetic dichroism of the two spin-orbit split multiplets can be derived within the nonrelativistic approximation from the coupling coefficients $C_{k_0}(j_0,K_f,J_f)$ and $C_{k_0}(j_0,J_f)$ in Eqs. (15) and (16). Only considering the lowest statistical tensor with $k_0=1$ and the properties of the $6j$ symbols, one can prove the validity of the following statement: The patterns of magnetic dichroism (with one zero crossing) in the two spin-orbit split multiplets in core-level photoelectron spectra are inverted with respect to each other. This means that within the nonrelativistic approximation one

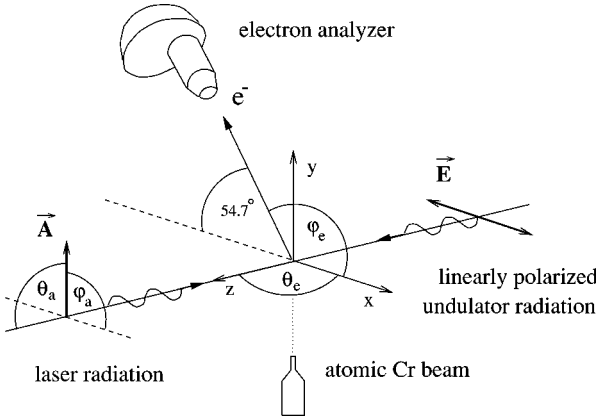

FIG. 1. Geometry of the experimental setup.

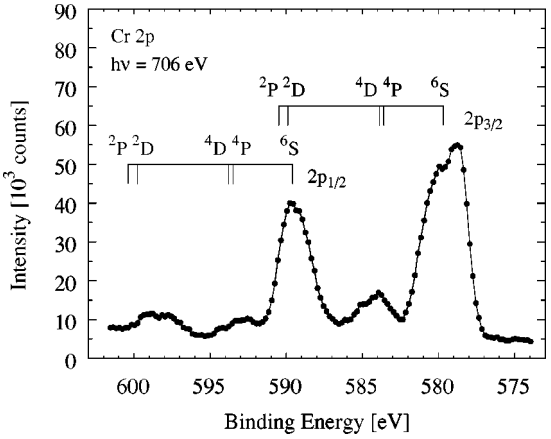

FIG. 2. Cr 2p photoelectron spectrum taken with 706 eV photons and with a total instrumental bandwidth of 1.4 eV. The bars displayed above the experimental spectrum indicate the calculated energies of LS terms with P and D symmetry for the configuration $3d^5$ relative to the ground state $3d^5(^6S)$ (see text).

gets a $+/-$ signature in the $j_0=l_0+1/2$ multiplet while a $-/+$ signature is predicted in the $j_0=l_0-1/2$ multiplet or vice versa [16].

III. EXPERIMENT

The LAD in the direct 2p photoionization of Cr atoms has been investigated at a photon energy of 706 eV. Free Cr atoms emanating in a collimated beam from a resistively heated furnace were aligned by pumping the optical transition Cr $3d^54s(^7S_3)\rightarrow 3d^54p(^7P_2)$ at $\lambda=42.909$ nm with linearly polarized laser radiation of about 100 mW. The laser radiation counterpropagated to the undulator radiation from beamline BW3 at HASYLAB, which was used to ionize the Cr atoms. The photoelectrons emitted close to the magic angle of 54.7° relative to the polarization axis of the undulator radiation were registered with the aid of a high-resolution Scienta SES 200 electron energy analyzer. The experimental setup is depicted schematically in Fig. 1. $\vec{E}$ denotes the electric field of the linearly polarized undulator radiation and $\vec{A}$ indicates the direction of the atomic polarization vector.

The geometry of the experimental setup determines the geometrical factors $F_{k_0kk_\gamma}$ [see Eq. (A1)] which depend on the emission direction of the photoelectrons (φ_e,θ_e), on the atomic polarization direction (φ_a,θ_a), and on the polarization of the ionizing photons. We assume the ionizing undulator radiation to be 100% linearly polarized. This assumption is well justified as demonstrated by the experimentally determined degree of polarization of $\geqslant 97\%$ [19]. The photoelectron emission direction is determined by the experimental setup and according to Fig. 1, we have $\varphi_e=180°-54.7°=125.3°$ and $\theta_e=90°$. The direction of the atomic polarization is varied. For pumping with linearly polarized laser radiation, $\vec{A}$ denotes the axis of the atomic alignment directed along the electric-field vector of the laser (φ_a is variable, $\theta_a=90°$). The explicit form for the coefficients $F_{k_0kk_\gamma}$ can be found in Ref. [11] as the particular geometry (for collinear photon beams) discussed there in Sec. 2.3 is equivalent to the one used here. In Table I in Ref. [11] the coefficients for $k_0=1,2$ are listed.[1]

The statistical tensors $\mathcal{A}_{k_00}$ in Eq. (A1) describe the polarization of the ground state of the atoms. Simulating the pumping process by solving the transition-rate equations approximate values for the $\mathcal{A}_{k_00}$ were obtained [20]. Depolarization effects due to atom-atom scattering and radiation trapping, as well as Doppler broadening have been taken into account. Only 84% of the Cr atoms (natural abundance of ^{52}Cr) could be pumped due to the isotope shift. Our calculations resulted in the values $\mathcal{A}_{20}\simeq 0.25$, $\mathcal{A}_{40}\simeq 0.07$, $\mathcal{A}_{60}\simeq 0.01$ for pumping with linearly polarized laser radiation. The calculations show that compared to the lowest statistical tensors $\mathcal{A}_{20}$ the higher orders are suppressed. Comparing the contributions of all terms of the sum in Eq. (A1) with $k_0=1,\ldots,6$ we found that only terms proportional to the atomic alignment $\mathcal{A}_{20}$ need to be taken into account in the theoretical description of the LAD in the Cr photoelectron spectra.

IV. RESULTS AND DISCUSSION

A. The 2p photoelectron spectrum of unpolarized Cr atoms

Figure 2 shows the 2p photoelectron spectrum of atomic Cr taken at a photon energy of 706 eV with a total instrumental bandwidth of 1.4 eV. The binding energies have been established using the well-known Cr 3d and rare-gas photoelectron lines. As expected from earlier studies of the 2p photoabsorption of atomic Cr [21], the photoelectron spectrum is dominated by the spin-orbit splitting of the 2p core hole. The two main photoelectron lines can therefore in a first attempt be assigned to the $2p_{1/2}$ line at higher binding energy and to the $2p_{3/2}$ line at lower binding energy. The 3d and the 4s valence electrons are assumed to be LS coupled

[1]It has to be noted that the coefficients F_{122}, F_{322}, and F_{342} in Table I in Ref. [11] have the wrong signs.

in the final ion, as in the ground state of the atom. This is justified by a single-configuration HF calculation for the Cr $2p$ photoionization performed in intermediate coupling. We used the suite of programs written by R. D. Cowan [13]. Only the configuration Cr $2p^6 3d^5 4s(^7S_3)$ for the initial state and Cr^+ $2p^5 3d^5 4s$ for the final state were taken into account. Further HF calculations verified that additional final-state configurations like $2p^5 3d^4 4s^2$ and $2p^5 3d^6$ do not significantly contribute. The spin-orbit parameters and the Slater integrals scaled down to 85% amount to (all values are given in eV):

$$\zeta(2p)=5.7,\ \xi(3d)=0.04,$$

$$F^2(2p,3d)=4.9,\ G^1(2p,3d)=3.5,\ G^3(2p,3d)=2.0,$$

$$F^2(3d,3d)=8.8,\ F^4(3d,3d)=5.5,$$

$$G^1(2p,4s)=0.2,\ G^2(3d,4s)=0.9. \qquad (18)$$

van der Laan and Kirkman calculated similar parameters in their study of the $2p$ absorption spectra of various $3d$-transition metal ions [22]. The $2p$ spin orbit parameter $\zeta(2p)$ and the Slater integrals of the Coulomb interactions between the $2p$ core hole and the $3d$ valence electrons $F^2(2p,3d)$ and $G^{1,3}(2p,3d)$ are of the same magnitude [Eq. (18)]. The spin-orbit splitting $\Delta E(2p_{1/2}-2p_{3/2})=3/2\,\zeta(2p)=8.6$ eV is larger than the expected multiplet splitting caused by the $2p$-$3d$ Coulomb interactions approximately equal to the values of the corresponding Slater integrals [13]. This justifies the preliminary assignment of the main lines to the jj coupled $2p_{1/2}^{-1}$ and $2p_{3/2}^{-1}$ hole introduced above.

The broad and asymmetric shape of the main lines can be explained by the combined effect of lifetime broadening and multiplet splitting due to the $2p$-$3d$ Coulomb interactions. This is treated in detail below. We focus here on an assignment of the main and satellite lines in Fig. 2 by considering the structure of the $3d$ valence shell. The spin-orbit interactions in the $3d$ shell can be neglected, but the strong $3d$ intra shell Coulomb interactions $F^{2,4}(3d,3d)$ need to be taken into account [Eq. (18)]. For the two main lines we assume the $3d$ shell to remain in the Hund's rule ground-state $3d^5(^6S)$ according to the LS coupling scheme. The satellites can be assigned to states where the $3d$ shell is recoupled. To demonstrate this we display the energy levels of possible LS terms of the configuration $3d^5$ for both the $2p_{1/2}$ and the $2p_{3/2}$ line as bar diagrams above the experimental spectrum in Fig. 2. The energies of the ^4P, ^4D and ^2P, ^2D states have been calculated relative to the Hund's rule ground-state $3d^5(^6S)$ with the aid of the $3d$-$3d$ Coulomb interaction matrix elements given in Ref. [23] together with the Slater parameters $F^{2,4}(3d,3d)$ from Eq. (18). The satellites between the main lines at 583–586 eV and the satellites between 592–594 eV can therefore be assigned to $2p_{3/2}^{-1}3d^5(^4P,\ ^4D)$ and $2p_{1/2}^{-1}3d^5(^4P,\ ^4D)$ states, respectively (Fig. 2). The satellites close to 598 eV may be assigned to $2p_{1/2}^{-1}3d^5(^2D,\ ^2P)$ states. In the binding energy region of the $2p_{1/2}$ line at 590 eV the energy levels of $2p_{1/2}^{-1}3d^5(^6S)$ states overlap with the levels of $2p_{3/2}^{-1}3d^5(^2D,\ ^2P)$ states. The Z+1 model based on the energy levels of Mn^+ $3d^5 4s$ or Fe^{2+} $3d^5 4s$ [24] results in a similar assignment of the satellites.

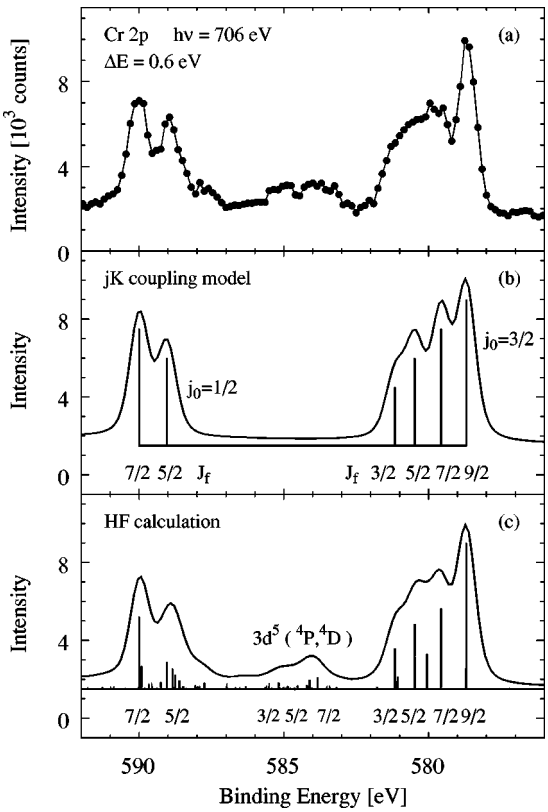

FIG. 3. (a) High-resolution Cr $2p$ photoelectron spectrum of the main lines binding-energy region taken with 706 eV photons and with a total instrumental bandwidth of 0.6 eV. (b) Bar diagram and convoluted line spectrum according to the jK coupling model (see text). (c) Bar diagram and convoluted line spectrum according to the HF calculation in intermediate coupling.

Figure 3(a) shows the Cr $2p$ photoelectron spectrum in the binding-energy region of the main lines taken with a total instrumental bandwidth of 0.6 eV at a photon energy of 706 eV. Due to the smaller energy bandwidth compared to the spectrum in Fig. 2, the multiplet structure of the Cr $2p$ main lines is partially resolved. This experimental spectrum will be interpreted with the aid of two different theoretical approaches. In Fig. 3(b), the result of a jK coupling model is depicted and in Fig. 3(c), the result of the single-configuration HF calculation is shown.

The jK coupling model comprises the single-configuration approximation with frozen valence shells, the jK coupling approximation, and the nonrelativistic approximation for the dipole matrix elements. These approximations have been introduced in Secs. II A and II C in order to simplify the theoretical description of dichroism in core-level photoelectron spectra. They can be used here for a determination of the relative cross sections of the unpolarized atoms without explicit knowledge of the dipole matrix elements. Within the above approximations the Cr $2p$ photoionization process reads

$$\hbar\omega + \mathrm{Cr}\, 2p^6 3d^5 4s(^7S_3) \rightarrow \mathrm{Cr}^+[2p^5(j_0 = 1/2,3/2)3d^5(^6S)4s(^7S_3)]J_f + \varepsilon s, \varepsilon d. \quad (19)$$

The $2p$-$3d$ Coulomb interactions couple the $2p$ hole described in jj coupling and the valence electrons described in LS coupling. Since we assume the valence electrons to have S symmetry in the final ion ($L_0 = 0$) the direct Coulomb interactions $F^2(2p,3d)$ do not cause any splitting ($j_0 = K_f$). The exchange Coulomb interactions $G^{1,3}(2p,3d)$ couple the core-hole total angular momentum $j_0 = 1/2,3/2$ and the total spin of the valence electrons $S_0 = 3$ to the total angular momentum of the ion J_f. This results in two fine-structure components $J_f = 7/2,5/2$ for the $j_0 = 1/2$ hole and in four fine-structure components $J_f = 3/2,5/2,7/2,9/2$ for the $j_0 = 3/2$ hole within the approximations.

The binding energies of these six fine-structure components given in the bar diagram in Fig. 3(b) were taken from the HF calculation. The energies of the six levels with the strongest $2p^{-1}_{1/2,3/2}3d^5 4s(^7S)$ eigenvector components were chosen. This approach promised to provide better binding energies than evaluating the exchange Coulomb interaction matrix elements for jK coupling. The HF energies had to be shifted by 0.87 eV towards lower binding energies in order to match the strongest photoelectron line in the experimental spectrum in Fig. 3(a) with the $J_f = 9/2$ fine-structure component. The length of the bars in Fig. 3(b) representing the relative cross section σ is proportional to the statistical weight of the fine-structure components $(2J_f + 1)$. [Within the above approximations, it is easy to show that $\sigma \propto (2J_f + 1)$].

To compare in more detail the result of the jK coupling model with the experimental result, a theoretical spectrum was calculated by replacing the bars by Lorentzian profiles of 0.3 eV full width at half maximum (FWHM) reflecting the lifetime of the $2p$ hole states [25]. The small difference between the lifetimes of the $2p_{1/2}$ and $2p_{3/2}$ hole states was neglected. The sum of the Lorentzian profiles was convoluted with a Gaussian profile of FWHM = 0.6 eV to account for the instrumental broadening and a linear background derived from a fit to the experimental spectrum was added. The result is shown as a solid curve in Fig. 3(b). The intensity is given in arbitrary units such as those for all other calculated spectra shown below. Although the main features of the Cr $2p$ photoelectron spectrum can be explained within the jK coupling model, the agreement between the experimental and the theoretical spectra is not satisfactory in detail: The relative intensity of the $2p_{1/2}$ multiplet and the intensity of the $J_f = 7/2$ and 5/2 components in the $2p_{3/2}$ multiplet are overestimated by the jK coupling model. The prominent satellites between the two multiplets are not reproduced.

The spectrum based on the binding energies and dipole amplitudes obtained by the single-configuration HF calculation in intermediate coupling is in much better agreement with the experimental results. The bars in Fig. 3(c) give the binding energies and the relative line intensities of the numerous multiplet components. The solid line was obtained in the same way as above in Fig. 3(b). The experimental and theoretical binding energies, the relative line intensities, and the assignments of the lines are summarized in Table I.

In the $2p_{3/2}$ multiplet, the four strongest HF lines [see bar diagram in Fig. 3(c)] can be assigned to $2p^{-1}_{3/2}3d^5(^6S)4s(^7S)$ states with $J_f = 9/2,\ 7/2,\ 5/2$, and 3/2. Their binding energies, which well correspond to the experimental values, have already been used for the jK coupling model spectrum in Fig. 3(b). The intensities of the $J_f = 7/2,\ 5/2$, and 3/2 lines are smaller according to the HF calculation than the statistical weight of the fine-structure components. Compared to the jK coupling model, the HF calculation predicts two additional lines at 580.1 and 581.1 eV with $J_f = 7/2$ and 5/2 in the $2p_{3/2}$ multiplet. They can be assigned to states with a recoupled 4s shell: $2p^{-1}_{3/2}3d^5(^6S)4s(^5S)$.[2] Although these lines cannot be observed directly in the experimental spectrum, their influence is very clear. According to the HF calculation, intensity is transferred from the four main lines to the two additional lines: The intensities in the $2p_{3/2}$ multiplet are redistributed giving rise to the characteristic spectral shape with one strong single peak and a broad and asymmetric structure at higher binding energies.

The redistribution of oscillator strength within the spectrum is caused by the admixture of different eigenvector components to the calculated HF energy levels. The strongest eigenvector components of some of the calculated energy levels are given in Table I. In the $2p_{3/2}$ multiplet, only the level with the lowest binding energy ($J_f = 9/2$) is a pure $2p^{-1}_{3/2}3d^5(^6S)4s(^7S)$ state. The other levels ($J_f = 7/2,5/2,3/2$) giving rise to the remaining three strong lines have dominant contributions of $2p^{-1}_{3/2}3d^5(^6S)4s(^7S)$ states but they contain significant admixtures of $2p^{-1}_{3/2}3d^5(^6S)4s(^5S)$ states with recoupled 4s shell.

The satellites between the two multiplets at 583–586 eV in the experimental spectrum are assigned to states with a recoupled 3d shell ($^4P,\ ^4D$) (see Table I, lines at 583.8, 584.1, and 585.2 eV with $J_f = 7/2,\ 5/2$, and 3/2). According to the HF calculation, intensity is transferred to these satellites from the $2p_{3/2}$ multiplet main lines through the mixture of states.

In the $2p_{1/2}$ multiplet, the lines are strongly mixed and an assignment is very difficult. But since the strongest eigenvector components are $2p^{-1}_{1/2}3d^5(^6S)4s(^7S)$ states (Table I) we call the high-binding energy multiplet $2p_{1/2}$ even though this cannot be unambiguously justified. The HF calculation predicts more lines in this energy region than the two fine-structure components of the jK coupling model. They are due to states with a $2p^{-1}_{3/2}$ hole and a recoupled 3d shell (^2L). This corroborates the conclusions drawn before in context with the discussion of Fig. 2. Similar to the $2p_{3/2}$ multiplet, the intensities in the $2p_{1/2}$ multiplet are redistributed.

[2]Only two of the expected four lines with $2p^{-1}_{3/2}3d^5(^6S)4s(^5S)$ have a considerable intensity since the two lines with $J_f = 3/2$ and 1/2 in LS-representation have strong admixtures of $2p^5 3d^5 4s(^4P)$ states, which are dipole-forbidden.

TABLE I. Binding energies, assignments, and relative intensities of the Cr $2p^6 3d^5 4s(^7S) \rightarrow Cr^+ 2p^5 3d^5 4s\,\varepsilon l$ photoelectron lines. The experimental binding energies were determined by a fit of the sum of Voigt profiles of 0.8 eV FWHM and a linear background to the measured spectrum. The assignments are based on the eigenvectors of the HF calculation in the jK coupling representation. The percentages give the weights of the strongest eigenvector components. The relative intensities are given following the result of the HF calculation and the jK coupling model (see text).

Binding energy (eV)		Assignment					Rel. int.	
Expt. ±0.5 eV	HF	J_f	j_0	Valence shells $3d^5$	$3d^5 4s$	%	HF	jK
578.7	578.7[a,b]	9/2	3/2	^6S	^7S	100	10	10
579.7	579.6 [b]	7/2	3/2	^6S	^7S	66	5.4	8
				^6S	^5S	31		
	580.1	7/2	3/2	^6S	^5S	67	2.3	
				^6S	^7S	27		
580.5	580.5 [b]	5/2	3/2	^6S	^7S	69	4.3	6
				^6S	^5S	17		
				^4D		3		
	581.1	5/2	3/2	^6S	^5S	72	0.8	
				^6S	^7S	12		
581.2	581.2 [b]	3/2	3/2	^6S	^7S	67	2.7	4
				^4D		17		
583.4	583.8	7/2	3/2	^4P		48	0.7	
584.1	584.1	5/2	3/2	^4D		28	0.6	
585.1	585.2	3/2	3/2	^4D		34	0.4	
587.8	587.7	5/2	3/2	^2S		25	0.4	
	588.6–588.9	5/2	3/2	^2L			2.9	
588.9	589.0 [b]	5/2	1/2	^6S	^7S	26	1.8	6
			3/2	^2D		20		
	589.2	7/2	3/2	^2F		19	0.4	
	589.9	7/2	3/2	^2G		25	1.5	
			1/2	^6S	^7S	18		
590.0	590.0 [b]	7/2	1/2	^6S	^7S	55	4.8	8
			3/2	^2G		5		

[a]The theoretical binding energy has been matched to the experimental value.
[b]The HF binding energies have been used as values for the jK coupling model.

Intensity is transferred from the main to the additional lines giving rise to the observed asymmetric line shape.

With the aid of the HF calculation we can trace back the discrepancies between the jK coupling model and the experimental spectrum to a deviation from the approximation of frozen valence shells. Recoupling in the valence $3d$ and $4s$ shells strongly influence the Cr $2p$ photoelectron spectrum, especially in the high binding energy region. An unambiguous assignment of the Cr $2p$ photoelectron lines in the high binding energy range of 588–590 eV to one value for the $2p$ hole total angular momentum j_0 and to one LS term for the valence shells is not possible. It has to be noted that the mixture of $2p_{1/2}^{-1}$ and $2p_{3/2}^{-1}$ states with the same valence-shell configuration such as $2p_{1/2}^{-1} 3d^5(^6S)4s(^7S)$ and $2p_{3/2}^{-1} 3d^5(^6S)4s(^7S)$ is negligibly small. The mixture of states thus mainly affects the high binding energy region of the Cr $2p$ photoelectron spectrum due to the overlap of the multitude of $2p_{3/2}^{-1} 3d^5(^2L)4s$ states with the $2p_{1/2}^{-1}$ states. Multiplet splitting and $3d$ valence-shell recoupling have also been observed in the $2p$ photoelectron spectra of Mn atoms [32] and Mn^{2+} ions [26].

B. Patterns and sum rules in the Cr 2*p* dichroism

Figure 4 shows the $2p$ photoelectron spectra of aligned Cr atoms taken at a photon energy of 706 eV with a total instrumental bandwidth of 1.4 eV. The $2p$ photoelectron spectra of oriented Cr atoms have been presented elsewhere [12]. The Cr atoms were aligned with linearly polarized laser radiation as described in Sec. III. The two photoelectron spectra shown in Fig. 4 correspond to two mutually perpendicular alignments of the atoms: parallel and perpendicular alignment with respect to the polarization axis of the linearly polarized undulator radiation (see Fig. 1 and Sec. III). The difference of the two spectra, i.e., the LAD, is displayed in Fig. 5(a). The LAD discussed in this section should, strictly speaking, be called LAD(0/90) to denote the angles of the axis of the atomic alignment $\varphi_a = 0°$ and $\varphi_a = 90°$ as defined in Fig. 1. We also measured the LAD(45/−45) which will be used in the next section in the discussion of the absolute scale of the dichroism effects. Since the LAD(0/90) is approximately two times larger than the LAD(45/−45) and therefore the signal-to-noise ratio is better, we will concen-

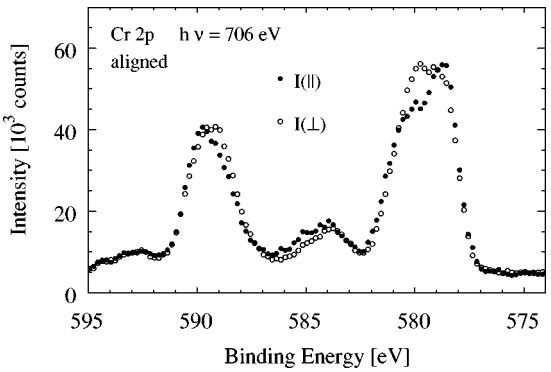

FIG. 4. The 2p photoelectron spectra of aligned Cr atoms for two perpendicular alignments of the atoms. The difference (LAD) is displayed in Fig. 5. Both spectra are taken with 706 eV photons and with a total instrumental bandwidth of 1.4 eV.

trate here on the discussion of the shape of the LAD(0/90) curve and call it LAD for brevity.

The LAD in the 2p photoelectron spectra of aligned Cr atoms is presented in Fig. 5(a). It clearly displays the characteristic LAD pattern with two zero crossings in the low binding energy $2p_{3/2}$ photoelectron line. This well corresponds to the predictions derived in Sec. II B. The existence of a strong LAD effect in the high binding energy line is in sharp contradiction to the nonrelativistic prediction stating that the LAD is equal to zero in the $2p_{1/2}$ line (Sec. II C). More insight in the origin of the LAD is achieved by comparing the experimental spectrum in Fig. 5(a) to the predictions of the jK coupling model in Fig. 5(b) and the HF calculation in Fig. 5(c).

Within the jK coupling model for atoms with S symmetry, the LAD is determined by the coupling coefficients $C_2(j_0,J_f)$ in Eq. (16). The length of the bars in Fig. 5(b) is proportional to the calculated values of the coefficients $C_2(j_0,J_f)$ for the different fine-structure components (these values are 0 for the components $J_f=7/2,5/2$ of the $2p_{1/2}$ multiplet, and $+25,-40,-9,+24$ $(\times[1/5\sqrt{2}])$ for $J_f=9/2,7/2,5/2,3/2$ in the $2p_{3/2}$ multiplet). From the bars, the solid line has been obtained as before. Figure 5(b) shows that the jK coupling model in respect to shape and sum rule describes the LAD in the $2p_{3/2}$ multiplet reasonably well, whereas in the $2p_{1/2}$ multiplet it completely fails.

The result of the HF calculation for the LAD is displayed in Fig. 5(c). Following the results in Sec. III only the statistical tensor $\mathcal{A}_{20}$ significantly contributes to the LAD. This reduces the number of terms in Eq. (A1) to four: for $k_0=2$ only the sets $(k_0kk_\gamma)=(220)$, (202), (222), and (242) are allowed. Evaluating the corresponding geometrical factors $F_{k_0kk_\gamma}$ and comparing the magnitude of the different parameters B_{220}, B_{202}, B_{222}, and B_{242} one finds that the contribution of B_{242} is approximately seven times larger than the contributions of the three other parameters. The shape of the LAD curve is thus mainly determined by the dominant parameter B_{242} in our experimental setup. The length of the bars in Fig. 5(c) correspond to the calculated values of the coefficients B_{242}. These have been calculated by inserting the HF dipole matrix elements $\langle \gamma_f J_f,\varepsilon lj:J\|D\|\gamma_0 J_0\rangle$ in the

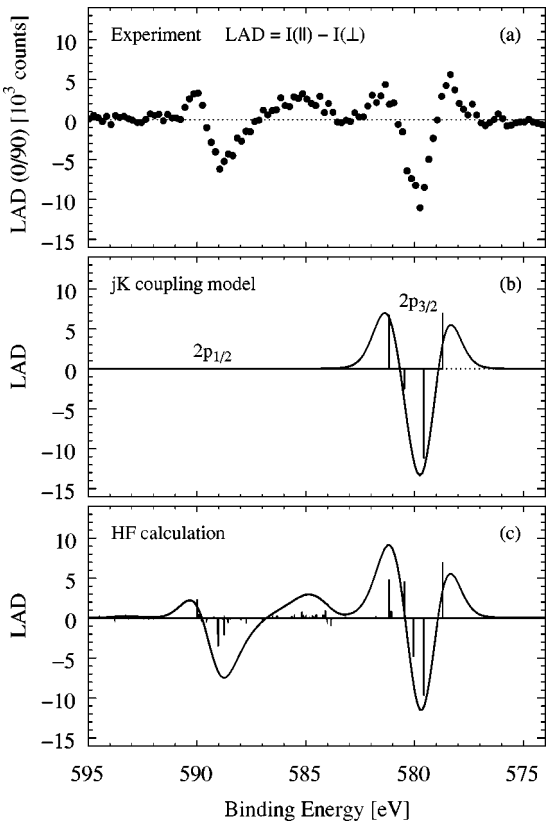

FIG. 5. (a) LAD in the 2p photoelectron spectra of aligned Cr atoms (difference spectrum of the two curves in Fig. 4). (b) LAD according to the jK coupling model (see text). (c) LAD as the result of the HF calculation in intermediate coupling.

expression for B_{242} given in Eq. (A3). Based on these values, the solid line was obtained as before. The HF calculation very well reproduces the main features of the experimental spectrum. A slight discrepancy at the high binding energy side of the $2p_{3/2}$ line is observed in form of a too strong positive lobe. The $2p_{3/2}$ satellites with recoupled 3d shell (^4P, ^4D) at around 585 eV show a strong positive LAD, in agreement with the experimental spectrum. In contrast, the $2p_{1/2}$ satellites with recoupled 3d shell (^4P, ^4D) close to 593 eV show almost no LAD. This agrees with the prediction of the jK coupling model that lines with $2p_{1/2}^{-1}$ hole do not show any LAD. According to the HF calculation, the strong LAD effect in the high binding energy main line is mainly due to the strong mixture of $2p_{1/2}^{-1}$ and $2p_{3/2}^{-1}$ states in this binding-energy region.

The LMDAD in the 2p photoelectron spectra of oriented Cr atoms has already been compared to the results of the intermediate coupling HF calculation [12]. This comparison is briefly summarized here with respect to the predictions of the jK coupling model. Both the shape and the relative sign of the Cr 2p LMDAD patterns with one positive and one negative lobe in both main photoelectron lines agree with the qualitative predictions in Sec. II [27]. Similar LMDAD patterns have been observed before in the 2p core-level photoelectron spectra of magnetized solid state samples [28–31,12] and a detailed comparison of the free atom Cr 2p LMDAD with the 2p LMDAD of a Cr surface layer is given

in Ref. [12]. The jK coupling model describes the general shape of the experimental LMDAD curve but details are not reproduced. Especially the sum rule stating that the LMDAD vanishes when integrated over each multiplet is not in agreement with the experimental observation [12]. The negative lobes in both multiplets are suppressed in the experimental spectrum (Fig. 1 in Ref. [12]) and the significant LMDAD outside the main lines is missing. With the HF calculation, we can trace back the deviation from the jK coupling model sum rule to the influence of the satellites with recoupled valence shells. Similar to the LAD, a strong mixture of $2p_{3/2}^{-1}3d^5(^2L)4s$ and $2p_{1/2}^{-1}3d^5(^6S)4s(^7S)$ states in particular explains the strong deviations in the high binding energy line.

In summary, the jK coupling model only yields a satisfactory description of the low binding energy $2p_{3/2}$ line, whereas at higher binding energies the jK coupling model fails. This can be explained with the aid of the HF calculation: In the low-binding-energy region of the Cr $2p$ photoelectron spectrum all features of the main line can be assigned to states with a $2p_{3/2}^{-1}$ hole. The assignment to one specific core-hole total angular momentum is a crucial approximation of the jK coupling model. Despite the influence of the satellites with recoupled valence shells, the LAD and LMDAD patterns in the $2p_{3/2}$ line persist as shown by the HF calculation. In the high-binding-energy main line, the situation is completely different since $2p_{1/2}^{-1}$ and $2p_{3/2}^{-1}$ core-hole states contribute. The strong LAD effect in the high-binding energy main line is a striking evidence for this. We conclude that only the assignment of the low-binding-energy Cr $2p$ photoelectron main line to $2p_{3/2}$ is justified and we expect a similar situation to be encountered in the $2p$ photoelectron spectra of the neighboring $3d$ metal atoms. Recent investigations on the $2p$ photoelectron spectra of Mn atoms [32] and Mn^{2+} ions [26] support this speculation.

C. Phase tilt and dipole amplitudes

The determination of the normalized dichroism allows for the evaluation of the generalized anisotropy coefficients $\beta_{k_0kk_\gamma}$, the ratio of the dipole amplitudes, and their phase difference. The LAD, i.e., the difference between two photoelectron spectra taken at mutually perpendicular alignments of the atoms, is given by

$$\mathrm{LAD}(\varphi_a/\varphi_a\pm 90°), I(\varphi_a)-I(\varphi_a\pm 90°) = K_{exp}\left(\frac{d\sigma}{d\Omega}(\varphi_a)-\frac{d\sigma}{d\Omega}(\varphi_a\pm 90°)\right), \tag{20}$$

where φ_a denotes the angle between the atomic alignment and the polarization axis of the ionizing undulator radiation (see Sec. III and Fig. 1) and the cross sections are given by Eq. (A1). The constant K_{exp} depends on experimental parameters, e.g., the atomic-beam density and the number of ionizing photons. Neglecting all higher orders except the atomic alignment $\mathcal{A}_{20}$ the sum of the two photoelectron spectra can be approximated by the cross section σ for unpolarized atoms: $I(\varphi_a)+2I(\varphi_a\pm 90°)\simeq K_{exp}3\sigma/4\pi$. Normalizing the LAD to this sum, the experimental parameters (K_{exp}), which are very difficult to determine, cancel out.

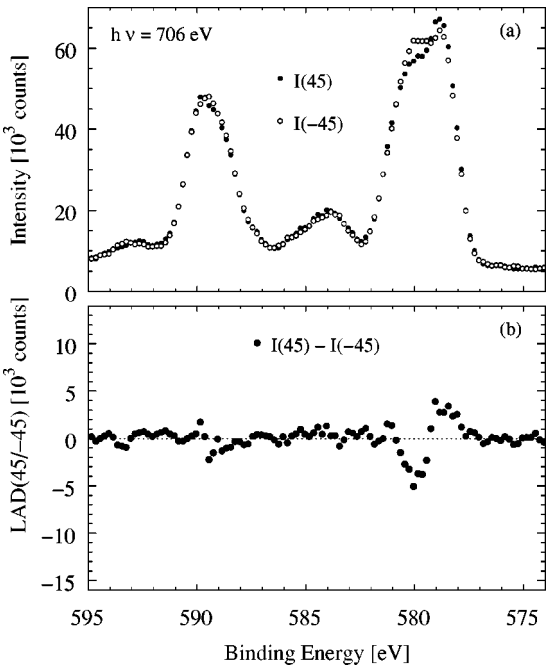

FIG. 6. (a) The $2p$ photoelectron spectra of aligned Cr atoms for the two perpendicular alignments of the atoms $\varphi_a=45°$ and $\varphi_a=-45°$ with respect to the polarization axis of the undulator radiation. Both spectra are taken with 706 eV photons and with a total instrumental bandwidth of 1.4 eV. (b) The difference of the two curves LAD$(45/-45)$.

The LAD(0/90) and the LAD$(45/-45)$ represent two independent measurable quantities since they are described by different linear combinations of the coefficients β_{2kk_γ} [20,33]. The LAD(0/90) was presented in Sec. IV B and the LAD$(45/-45)$ is depicted in Fig. 6. The experimental determination of the parameters β_{2kk_γ} from the normalized LAD spectra is hampered by the fact that we cannot measure the atomic alignment $\mathcal{A}_{20}$. It is therefore advantageous to determine the so-called "phase tilt" [33,7,8]

$$\tan 2\delta^{tilt}=\frac{I(45°)-I(-45°)}{I(0°)-I(90°)} \tag{21}$$

which is independent of the magnitude of the atomic alignment. Experimentally, the angle δ^{tilt} is equal to the angle φ_a^{max} for which the photoelectron intensity reaches its maximum [33]. The $\tan 2\delta^{tilt}$ is given by [see, also, Eq. (25) in Ref. [33]]

$$\tan 2\delta^{tilt}=\frac{8\sqrt{7}\sin 2\varphi_e\beta_{220}+8\sqrt{5}\sin 2\varphi_e\beta_{222}-(10\sin 2\varphi_e+35\sin 4\varphi_e)\beta_{242}}{8\sqrt{7}\cos 2\varphi_e\beta_{220}-8\sqrt{14}\beta_{202}+8\sqrt{5}(1+\cos 2\varphi_e)\beta_{222}-(3+10\cos 2\varphi_e+35\cos 4\varphi_e)\beta_{242}}. \quad (22)$$

Within the approximations of the jK coupling model for the Cr 2p photoionization the parameters $\beta_{k_0kk_\gamma}$ take the form [Eqs. (A2), (14), (16), and (17)]

$$\beta_{k_0kk_\gamma}=\sqrt{3}\,\frac{C_{k_0}(j_0,J_f)b_{k_0kk_\gamma}}{C_0(j_0,J_f)b_{000}}=3\frac{C_{k_0}(j_0,J_f)b_{k_0kk_\gamma}}{(2J_f+1)(D_s^2+D_d^2)}. \quad (23)$$

Inserting these expressions in Eq. (22) the coupling coefficients $C_{k_0}(j_0,J_f)$ cancel out. This results in a phase tilt independent of the angular momenta j_0 and J_f. The dipole matrix elements $\langle \varepsilon l\|d\|l_0\rangle$ are defined in analogy to the definitions in [34] as:

$$\langle \varepsilon l\|d\|l_0\rangle=D_l e^{i\Delta_l}, \quad (24)$$

$$D_l=(-1)^{l_0-[(l_0+l-1)/2]}\sqrt{\frac{l_0+l+1}{2}}\int_0^\infty P_{l_0}(r)rP_{\varepsilon l}(r)dr, \quad (25)$$

$$\Delta_l=\sigma_l+\delta_l-\frac{l\pi}{2}, \quad (26)$$

with the radial wave functions $P_{\varepsilon l}(r)=rR_{\varepsilon l}(r)$. The phase shifts Δ_l contain the phase shifts due to the long-range Coulomb potential σ_l, to the short-range atomic potential δ_l, and to the centrifugal potential $l\pi/2$ [34]. In the following, we compare the experimentally determined phase-tilt for the Cr 2p photoionization at a photon energy of 706 eV with the results of the jK coupling model and the HF calculation. We concentrate on the $J_f=9/2$ line with the lowest binding energy of 578.7 eV (Table I) since it is least disturbed by other photoelectron lines. From a fit of Gaussian profiles to the 2p photoelectron lines in Fig. 4 for $\varphi_a=0°,90°$ and in Fig. 6(a) for $\varphi_a=45°,-45°$, and to the lines in the LAD(0/90) and LAD(45/−45) spectra [Figs. 5(a) and 6(b)] the angle δ^{tilt} could be determined at 706 eV according to Eq. (21) to:

$$\delta^{tilt}=15°\pm 10°. \quad (27)$$

For the fit of the 2p photoelectron spectra a linear background has been taken into account. The width of the Gaussians (FWHM 1.4 eV) well corresponds to the expected experimental bandwidth of 1.4 eV.

The ratio of the dipole amplitudes and phase difference calculated within the single-configuration HF calculation in intermediate coupling for a photon energy of 706 eV are

$$D_s/D_d=-0.173, \quad (28)$$

$$\Delta_s-\Delta_d=-63°\pm 5°, \quad (29)$$

with the amplitude for transitions to outgoing d waves being approximately six times larger than to s waves. The uncertainty of the phase difference is due to numerical reasons. Using these values, the phase tilt has been calculated in the jK coupling model with Eqs. (21)–(25). The calculation yields $\delta^{tilt}=5°\pm 3°$ consistent with the experimental value. This is further supported by the fact that with the β_{2kk_γ} parameters determined by the HF calculation in their general form in Eqs. (A2) and (A3), Eq. (22) yields $\delta^{tilt}=4.4°$ in excellent agreement with the above value obtained within the jK coupling model. The $J_f=9/2$ line in the Cr 2p photoelectron spectrum can be described by the jK coupling model whereas for the other photoelectron lines at higher binding energies, an experimental determination of the phase tilt with the aid of the jK coupling model is not meaningful since the lines are strongly mixed (see Sec. IV B).

The experimental value of the angle δ^{tilt} results within the jK coupling model in the following restriction for the phase difference: $\cos(\Delta_s-\Delta_d)>0$ [with Eqs. (16, (17), and (22)–(26)]. The sign of the LMDAD on the other hand requires that $\sin(\Delta_s-\Delta_d)<0$ [20]. These two requirements restrict the values for the phase difference to $-90°<\Delta_s-\Delta_d<0°$ consistent with the result of the HF calculation.

V. SUMMARY

We have developed a pure angular momentum coupling model for a qualitative description of dichroism in deep core-level photoelectron spectra assuming the single configuration, the frozen valence shells, and the jj or jK coupling approximations. A product form for the dynamical coefficients $B_{k_0kk_\gamma}$ allowed for the derivation of simple dichroism patterns and sum rules for the dichroism. The model also gives access to the dipole amplitudes and phase difference of the dipole matrix elements. It is applied in the present paper to the analysis of the Cr 2p photoionization process.

The 2p photoelectron spectrum of unpolarized Cr atoms exhibits a complex fine structure that allowed for a detailed investigation of the multiplet splitting in the final ion. The importance of both the 2p spin-orbit interaction and of the Coulomb interactions between the 2p core hole and the 3d valence electrons has been demonstrated. The recoupling of the 3d and 4s valence shells was shown to strongly influence the Cr 2p photoelectron spectrum. The results were obtained by comparing the experimental spectrum to the results of the jK coupling model and HF calculations in intermediate coupling. The validity of both approaches was further tested by investigating the spectral shapes (patterns) and the integrated dichroism (sum rules) of the LAD in the 2p photoelectron spectra of aligned Cr atoms, respectively. The LAD displays the characteristic pattern with two zero crossings only in the low binding energy 2$p_{3/2}$ main photoelectron line. The

strong LAD effect in the high-binding-energy main line is a striking evidence for the contribution of $2p_{1/2}^{-1}$ *and* $2p_{3/2}^{-1}$ core-hole states to the high-binding-energy main line. The origin of the LAD and LMDAD [12] patterns could be explained accounting for the angular momentum coupling and the multiplet splitting in the final ion. Deviations from the jK coupling sum rule stating that the dichroism vanishes when integrated over each main line could be traced back to the recoupling of the $3d$ and $4s$ valence shells. Both LAD and LMDAD [12] experimental spectra are well described by the HF calculation in intermediate coupling. Evaluating the normalized dichroism, a consistent set of parameters for the dipole amplitudes and for the phase difference describing the dynamics of the Cr $2p$ photoionization process could be determined.

Our experimental and theoretical investigations on the Cr $2p$ photoelectron spectrum can serve as a basis for the discussion of the $2p$ photoelectron and $2p$ dichroism spectra of $3d$ transition-metal atoms in general. Multiplet splitting due to the $2p$-$3d$ Coulomb interactions and valence shell recoupling are expected to strongly influence the $2p$ photoelectron and $2p$ dichroism spectra of other $3d$ metal atoms. This is confirmed by a recent investigation of the $2p$ photoelectron spectrum of unpolarized Mn atoms [32]. The interpretation of the $2p$ photoelectron spectra of bound $3d$ transition-metal atoms may also benefit from our study. Intra-atomic interactions can dominate the $2p$ photoelectron spectra of $3d$ metal atom compounds and thin films. This is shown in the comparison of the $2p$ photoelectron spectra of free Mn atoms and MnO [32] and in the comparison of the LMDAD spectra of free oriented Cr atoms and a magnetized Cr surface layer [12].

ACKNOWLEDGMENTS

The help of A. Verweyen during the beamtime is gratefully acknowledged. We thank the Deutsche Forschungsgemeinschaft for financial support and the HASYLAB staff for continuous assistance. N.M.K. acknowledges the hospitality of Bielefeld University.

APPENDIX

The cross section for the photoionization of polarized atoms can be presented in the general form [11]

$$\frac{d\sigma}{d\Omega}=\frac{\sigma}{4\pi}\left(1+\sum_{k_0kk_\gamma}\mathcal{A}_{k_00}F_{k_0kk_\gamma}\beta_{k_0kk_\gamma}\right). \tag{A1}$$

The summation is performed over all possible sets (k_0kk_γ) except (000). The reduced statistical tensors $\mathcal{A}_{k_00}$ with rank $k_0=0,1,\ldots,2J_0$ describe the polarization of the initial state of the atom and the geometrical factors $F_{k_0kk_\gamma}$ describe the geometry of the experimental setup. The generalized anisotropy coefficients $\beta_{k_0kk_\gamma}$ contain the dipole amplitudes and describe the dynamics of the photoionization process. They are of the form

$$\beta_{k_0kk_\gamma}=\sqrt{3}\,\frac{B_{k_0kk_\gamma}}{B_{000}}, \tag{A2}$$

where the coefficients $B_{k_0kk_\gamma}$ are given by [11]

$$\begin{aligned}B_{k_0kk_\gamma}=3\hat{J}_0\sum_{\substack{JJ'\\ ll'jj'}}(-1)^{J+J_f+k_\gamma-1/2}\hat{J}\hat{J}'\hat{j}\hat{j}'\hat{l}\hat{l}'(l0,l'0|k0)\\ \times\begin{Bmatrix} j & l & \frac{1}{2}\\ l' & j' & k\end{Bmatrix}\begin{Bmatrix} j & J & J_f\\ J' & j' & k\end{Bmatrix}\begin{Bmatrix} J_0 & 1 & J\\ J_0 & 1 & J'\\ k_0 & k_\gamma & k\end{Bmatrix}\\ \times\langle\alpha_fJ_f,\varepsilon lj{:}J\|D\|\alpha_0J_0\rangle\langle\alpha_fJ_f,\varepsilon l'j'{:}J'\|D\|\alpha_0J_0\rangle^*.\end{aligned} \tag{A3}$$

Here, J_0, α_0 (J_f,α_f) characterize the initial (final) state of the atom (ion), lj are the orbital and total angular momenta of the photoelectron, and $\langle\alpha_fJ_f,\varepsilon lj{:}J\|D\|\alpha_0J_0\rangle$ are the multi-channel dipole amplitudes. The standard notations for the Clebsch-Gordan coefficients and the Wigner nj coefficients are used and $\hat{J}\equiv(2J+1)^{1/2}$. The angle-integrated photoionization cross section of unpolarized atoms is determined by

$$\begin{aligned}\sigma&=\frac{4\pi^2\alpha\omega}{3(2J_0+1)}\sum_{ljJ}|\langle\alpha_fJ_f,\varepsilon lj{:}J\|D\|\alpha_0J_0\rangle|^2\\ &=\frac{4\pi^2\alpha\omega}{3\sqrt{3}(2J_0+1)}B_{000},\end{aligned} \tag{A4}$$

where ω is the frequency of the ionizing photon and α is the fine-structure constant.

Any dichroism discussed here is defined as the difference of cross sections for two different directions of the polarization of the target atom and, therefore, is described by terms with $k_0>0$ in the general expression for the cross section Eq. (A1) [2]. Only terms proportional to odd statistical tensors $\mathcal{A}_{10},\mathcal{A}_{30},\ldots$ contribute to CMD and LMDAD, i.e., the magnetic dichroism is determined by the atomic orientation. The linear alignment dichroism LAD is determined by the atomic alignment, as only terms proportional to even statistical tensors $\mathcal{A}_{20},\mathcal{A}_{40},\ldots$ contribute [2].

[1] N. A. Cherepkov, V. V. Kuznetsov, and V. A. Verbitskii, J. Phys. B **28**, 1221 (1995).

[2] A. Verweyen, A. N. Grum-Grzhimailo, and N. M. Kabachnik, Phys. Rev. A **60**, 2076 (1999).

[3] A. von dem Borne, T. Dohrmann, A. Verweyen, B. Sonntag, K. Godehusen, and P. Zimmermann, Phys. Rev. Lett. **78**, 4019 (1997).

[4] A. von dem Borne, Th. Dohrmann, A. Verweyen, B. Sonntag, K. Godehusen, P. Zimmermann, and N. M. Kabachnik, J. Phys. B **31**, L41 (1998).

[5] A. von dem Borne, R. L. Johnson, B. Sonntag, M. Talkenberg, A. Verweyen, Ph. Wernet, J. Schulz, K. Tiedtke, Ch. Gerth, B. Obst, P. Zimmermann, and J. E. Hansen, Phys. Rev. A **62**, 052703 (2000).

[6] A. Verweyen, Ph. Wernet, B. Sonntag, K. Godehusen, and P. Zimmermann, J. Electron Spectrosc. Relat. Phenom. **101–103**, 179 (1999).

[7] A. Verweyen, Ph. Wernet, J. Schulz, B. Sonntag, M. Martins, K. Godehusen, and P. Zimmermann, J. Phys. B **32**, 4079 (1999).

[8] K. Godehusen, P. Zimmermann, A. Verweyen, A. von dem Borne, Ph. Wernet, and B. Sonntag, Phys. Rev. A **58**, R3371 (1998).

[9] K. J. Ross and B. Sonntag, Rev. Sci. Instrum. **66**, 4409 (1995).

[10] Th. Dohrmann, A. von dem Borne, A. Verweyen, B. Sonntag, M. Wedowski, K. Godehusen, and P. Zimmermann, J. Phys. B **29**, 5699 (1996).

[11] S. Baier, A. N. Grum-Grzhimailo, and N. M. Kabachnik, J. Phys. B **27**, 3363 (1994).

[12] Ph. Wernet, J. Schulz, B. Sonntag, K. Godelhusen, P. Zimmermann, M. Martins, C. Bethke, and F. U. Hillebrecht, Phys. Rev. B **62**, 14 331 (2000).

[13] R. D. Cowan, *The Theory of Atomic Structure and Spectra* (University of California Press, California, 1981).

[14] I. I. Sobelman, *Introduction to the Theory of Atomic Spectra* (Pergamon Press, New York, 1972).

[15] D. A. Varshalovich, A. N. Moskalev, and V. K. Khersonskii, *Quantum Theory of Angular Momentum* (World Scientific, Singapore, 1988).

[16] B. T. Thole and G. van der Laan, Phys. Rev. B **44**, 12 424 (1991); G. van der Laan, Phys. Rev. Lett. **66**, 2527 (1991); B. T. Thole and G. van der Laan, *ibid.* **70**, 2499 (1993).

[17] K. Mitsuke, Y. Hikosaka, and K. Iwasaki, J. Phys. B **33**, 391 (2000).

[18] N. A. Cherepkov and V. V. Kuznetsov, J. Phys. B **22**, L405 (1989).

[19] R. Wehlitz, B. Langer, N. Berrah, S. B. Whitfield, J. Viefhaus, and U. Becker, J. Phys. B **26**, L783 (1993).

[20] Ph. Wernet, Ph.D. thesis, Universität Hamburg, 2000.

[21] U. Arp, K. Iemura, G. Kutluk, T. Nagata, S. Yagi, and A. Yagishita, J. Phys. B **28**, 225 (1995).

[22] G. van den Laan and I. W. Kirkman, J. Phys.: Condens. Matter **4**, 4189 (1992).

[23] C. W. Nielson and G. F. Koster, *Spectroscopic Coefficients for the pn, dn, and fn Configurations* (MIT Press, Cambridge, MA, 1963).

[24] J. Sugar and C. Corliss, J. Phys. Chem. Ref. Data **14**, 115 (1985).

[25] M. O. Krause and J. H. Oliver, J. Phys. Chem. Ref. Data **8**, 329 (1979).

[26] P. S. Bagus, R. Broer, W. A. de Jong, W. C. Nieuwpoort, F. Parmigiani, and L. Sangaletti, Phys. Rev. Lett. **84**, 2259 (2000).

[27] Within the approximations of the *jK* coupling model, the coupling coefficients $C_1(j_0,J_f)$ in Eq. (16) determine the shape of the LMDAD curve. The coefficients $C_1(j_0,J_f)$ take the calculated values $+8,-8$ $(\times[1/\sqrt{2}])$ for the fine-structure components $J_f=7/2,5/2$ of the $2p_{1/2}$ multiplet and the values $+15,0,-7,-8$ $(\times[1/\sqrt{2}])$ for the components $J_f=9/2,7/2,5/2,3/2$ of the $2p_{3/2}$ multiplet. The shape of the experimental LMDAD thus agrees with the rule of inverted LMDAD signals for lines with different core hole total angular momentum found in Sec. II C.

[28] F. U. Hillebrecht, Ch. Roth, H. B. Rose, W. G Park, E. Kisker, and N. A. Cherepkov, Phys. Rev. B **53**, 12 182 (1996).

[29] D. Knabben, Th. Koop, H. A. Dürr, F. U. Hillebrecht, and G. van der Laan, J. Electron Spectrosc. Relat. Phenom. **86**, 201 (1997), and references therein.

[30] G. Rossi, G. Panaccione, F. Sirotti, S. Lizzit, A. Baraldi, and G. Paolucci, Phys. Rev. B **55**, 11 488 (1997).

[31] S. H. Baker, K. W. Edmonds, A. M. Keen, S. C. Thornton, C. Norris, and C. Binns, Phys. Rev. B **61**, 5026 (2000).

[32] Ph. Wernet, B. Sonntag, M. Martins, P. Glatzel, B. Obst, and P. Zimmermann, Phys. Rev. A **63**, 050702(R) (2001).

[33] M. Wedowski, K. Godehusen, F. Weisbarth, P. Zimmermann, M. Martins, Th. Dohrmann, A. von dem Borne, B. Sonntag, and A. N. Grum-Grzhimailo, Phys. Rev. A **55**, 1922 (1997).

[34] A. F. Starace, *Theory of Atomic Photoionization*, edited by W. Melhorn, Handbuch der Physik Vol. 31 (Springer-Verlag, Berlin, 1982).